分级孔 rGO/NiO 的异质自组装制备及其电化学性能

袁淑霞[1,2]， 杨明珲[3]， 吕春祥[2]， 王晓敏[1]

（1. 太原理工大学，山西 太原 030024；
2. 中国科学院山西煤炭化学研究所，炭材料重点实验室，山西 太原 030001；
3. 航天材料及工艺研究所，北京 100076）

摘 要： 采用异质自组装法制备得到氧化石墨烯/$Ni(HCO_3)_2$（GO/$Ni(HCO_3)_2$），经热还原分解后得到石墨烯/NiO（rGO/NiO）。通过 XRD、SEM 和 N_2 吸脱附测试等手段详细研究了 GO/$Ni(HCO_3)_2$ 向 rGO/NiO 转变过程中的结构变化，结果表明，rGO/NiO 的比表面积和孔容分别为 121.3 $m^2\ g^{-1}$ 和 0.26 $cm^3\ g^{-1}$，呈分级孔分布，孔径主要分布为 2～100 nm。大的比表面积和分级孔的分布使得 rGO/NiO 呈现出优异的电化学性能。在 0.5 A g^{-1} 的电流密度下比电容是 919 F g^{-1}。当电流密度从 0.5 A g^{-1} 提高至 5 A g^{-1} 时，比电容保持率为 71%。长周期循环稳定性结果显示，在 2 A g^{-1} 的电流密度下循环 3 000 次后比电容保持率为 91%。

关键词： 异质自组装；分级孔；rGO/NiO；电化学性能

中图分类号： TB33 **文献标识码：** A

基金项目：国家自然科学基金（51572184）.

通讯作者：王晓敏，博士，教授. E-mail：wangxiaomin@tyut.edu.cn

Synthesis of a rGO/NiO composite with a hierarchical pore structure by self-assembly and its electrochemical performance as a supercapacitor electrode

YUAN Shu-xia[1,2], YANG Ming-hui[3], LU Chun-xiang[2], WANG Xiao-min[1]

(1. *Taiyuan University of Technology*, *Taiyuan* 030024, *China*;
2. *Key Laboratory of Carbon Materials*, *Institute of Coal Chemistry*, *Chinese Academy of Sciences*, *Taiyuan* 030001, *China*;
3. *Aerospace Research Institute of Materials & Processing Technology*, *Beijing* 100076, *China*)

Abstract: A GO/$Ni(HCO_3)_2$ composite was synthesized by the self-assembly of layer $Ni(HCO_3)_2$ and GO in a mixed suspension under sonication, followed by heat treatment to obtain rGO/NiO for use as the electrode material of supercapacitors. The structural change from the GO/$Ni(HCO_3)_2$ to the rGO/NiO was investigated by XRD, SEM, and nitrogen adsorption. Results indicate that the rGO/NiO has a specific surface area of 121.3 $m^2\ g^{-1}$ and pore volume of 0.26 $cm^3\ g^{-1}$, and a hierarchical porous structure with a pore size range of 2-100 nm. The high specific surface area and the hierarchical porous structure give the rGO/NiO composite a high specific capacitance of 919 F g^{-1} (0.5 A g^{-1}) and an excellent rate capability with a capacitance retention rate of 71% when the current density increases from 0.5 to 5 A g^{-1}. The specific capacitance retains 91% of its original value after cycling at a current density of 2 A g^{-1} for 3 000 cycles, indicating good stability.

Key words: Heterogeneous assembly; Hierarchical porous; rGO/NiO; Electrochemical performance

Received date: 2020-05-06; *Revised date*: 2020-06-16

Foundation item: National Natural Science Foundation of China (51572184).

Corresponding authors: WANG Xiao-min, Ph. D. Professor. E-mail: wangxiaomin@tyut.edu.cn

1 Introduction

The coming of energy crises and growing environmental problems have inspired considerable attention in the development of clean and renewable energy sources[1-4]. Supercapacitors are the most promising candidates for next-generation energy storage devices owing to their high power density, fast charge/discharge features, long cycle life, low maintenance cost, eco-friendliness and high safety[5-9]. Among the various pseudo-capacitive materials investigated, nickel oxide (NiO) has attracted great interest owing

to its high redox activity, cost effectiveness, eco-friendliness, natural abundance and outstanding theoretical capacity of 2 584 F g^{-1}[10, 11]. However, NiO exhibits a poor electronic conductivity (~10^{-4} S cm^{-1}), low accessible surface areas, and strain formation during the charge-discharge processes, which limit its rate capability, long-term stability and power density[12, 13].

To overcome these issues, its combinations with different carbonaceous materials have been studied. Liu et al[14, 15] designed and constructed an electrode material with a hierarchical shell-core structure by anchoring NiO nanospines on concave spherical carbon particles. The as-synthesized electrode exhibited superior electrochemical performance with a high specific capacitance (1 161 F g^{-1} at a high current density of 2 A g^{-1}), a good rate capability (839 F g^{-1} at a high current density of 10 A g^{-1}) as well as long cycling stability (92.4% retention rate after 3 000 cycles at a high current density of 2 A g^{-1}). Nunes et al[16] reported an electrode material for supercapacitors composed of NiO nanoparticles supported onto radially oriented multi-walled carbon nanotubes (CNTs) using a stainless-steel fine-mesh as the support (AISI: CNT-NiO). A specific capacitance of 1 028 F g^{-1} was obtained at a scan rate of 0.02 V s^{-1}. More recently, graphene has attracted researcher's interest owing to its two-dimensional hexagonal network, high electronic conductivity, enhanced mechanical strength, and improved specific surface area. Yus et al[15] proposed a hetero-coagulation route to prepare a rGO/NiO hybrid structure. In a first step, as-synthesized NiO and rGO formed a core-shell structure by electrostatic interaction in the adequate ratio, in which polyelectrolyte was used as a ligand. Then, the resulting rGO/NiO composite was shaped using electrophoresis deposition (EPD) in order to fully cover the 3D Ni foam substrates, after which a subsequent mild thermal treatment process was applied. The hybrid exhibited excellent performance with a high specific capacitance of 940 F g^{-1} and a high rate capability at a current density of 2 A g^{-1}. The hetero-coagulation method can be described as follows. The layered double hydroxides with a positive charge and the two dimension graphene oxide (GO) with a negative charge were exfoliated into single layer nanosheets in water by liquid-phase exfoliation. And then, these nanosheets were assembled by layer-by-layer assembly under mutual electrostatic interactions[17, 18].

Recently, $Ni(HCO_3)_2$ has attracted the attention of researchers due to its enhanced electrochemical performances[19, 20]. Tian et al[21] developed a facile and efficient route to prepare a $Ni(HCO_3)_2$/polydopamine/rGO composite. The as-prepared composite offered a high Faradaic capacity of 870 C g^{-1} at 0.5 A g^{-1} and a moderate rate capability. The assembled asymmetric supercapacitor delivered a specific capacity of 192 C g^{-1} at 0.5 A g^{-1} within an operation voltage window of 1.7 V. The maximum energy density reached to 45.3 Wh kg^{-1} at a power density of 425 W kg^{-1}, and the initial specific capacity maintained 90.5% after 3 000 times charge-discharge cycles. $Ni(HCO_3)_2$, a new type of two-dimensional nanomaterial, can also be exfoliated into single layer nanosheets in water by liquid-phase exfoliation. More importantly, CO_2 and H_2O produced might affect the structure of the materials during the transformation from $Ni(HCO_3)_2$ to NiO, leading to enhanced electrochemical performance.

In this work, rGO/NiO was fabricated by the heterogeneous assembly of GO and $Ni(HCO_3)_2$ and thermal treatment. The changes of the structure from GO/$Ni(HCO_3)_2$ to rGO/NiO were studied. Finally, the electrochemical performances of rGO/NiO were evaluated in terms of the capacitance, the rate performance, and the long-term cycling stability.

2 Experimental

2.1 Materials

All chemicals employed were of analytical grade. Nickel chloride was purchased from Shanghai Aladdin Biochemistry Technology Co., Ltd. Urea was purchased from TianDa Chemical Reagent Co. Potassium hydroxide, polytetrafluoro-ethylene emulsion (PTFE, 60 wt.%), and acetylene black were purchased from Sinopharm Chemical Reagent Co. Ltd. Graphene oxide (GO) was provided by the key Laboratory of Carbon Materials, Institute of Coal Chemistry, Chinese Academy of Sciences.

2.2 Synthesis of $Ni(HCO_3)_2$

$Ni(HCO_3)_2$ was synthesized by an one-step hydrothermal method. Typically, 0.57 g $NiCl_2 \cdot 6H_2O$ and 1.441 g urea were dissolved in 60 mL deionized water, followed by magnetically stirring for 30 min to form a homogeneous solution. The mixture solution was transferred into a 100 mL Teflon-lined autoclave and kept at 160 °C for 12 h. The resulting products were separated by a suction filtration, washed with distilled water, and then dried at 60 °C for 24 h.

2.3 Synthesis of the rGO /NiO composite

Firstly, 0.25 g $Ni(HCO_3)_2$ was dispersed in 800 mL DI water by mechanical stirring, followed by ultrasonication (bath sonicator, 50 Hz, 3 h) to obtain a colloidal suspension of $Ni(HCO_3)_2$. Next, the colloidal suspension was mixed with 15 mL (1.2 mg

mL^{-1}) GO colloidal suspension and sonicated for 30 min under mechanical stirring for 16 h. GO/Ni $(HCO_3)_2$ was obtained by vacuum filtration, followed by washing and drying. Finally, as-prepared GO/Ni$(HCO_3)_2$ was annealed at 300 °C for 4 h under the atmosphere of Ar and the rGO /NiO composite was obtained.

2.4 Characterization

The morphology of the materials was investigated by field emission scanning electron microscopy (FESEM, JSM-7001F). Phase structures were characterized by X-ray diffraction (XRD, Bruker D8 Advance) with Cu Ka radiation (λ = 0.154 06 nm). Thermogravimetric analysis (TG) was performed using a Mettler TGA2 instrument, under air flow with a heating rate of 10 °C min^{-1} from room temperature to 800 °C. The specific surface area and pore structure were characterized by N_2 adsorption/desorption isotherms at 77 K (Micromeritics, ASAP-2020). The specific surface areas were obtained using the Brunauer Emmett Teller (BET) method and the pore size distributions were analyzed by the Barrett Joyner Halenda (BJH) model. Electrochemical studies were carried out using a three-electrode configuration. A platinum foil and Hg/HgO were used as the counter and reference electrode, respectively. The working electrode was prepared by mixing the active material, acetylene black, and PTFE in a weight ratio of 85∶10∶5. The obtained slurry was uniformly pasted on a nickel foam and the average weight of the mixed materials on each electrode was about 3-5 mg. The prepared electrode was dried at 60 °C for 24 h and then pressed at 10 MPa.

2.5 Electrochemical measurements

Cyclic voltammetry (CV), galvanostatic charge/discharge (CD) and electrochemical impedance spectroscopy (EIS) measurements were carried out on a CHI 660E electrochemical working station (Shanghai Chenhua Apparatus CO., Ltd.) with 2 mol L^{-1} KOH as an electrolyte. The EIS data were recorded in the frequency range from 0.1 Hz to 100 kHz with an excitation signal of 5 mV at the open circuit potential. The charge-discharge cycling tests were performed on a Land-CT2001A instrument, in the 0-0.6 V potential range. The specific capacitances were calculated from the discharging curves using the following equations:

$$C = \frac{I\Delta t}{M\Delta V} \quad (1)$$

Where C (F g^{-1}) represents the specific capacitance, I (A) is the discharge current, Δt (s) is the discharge time, m (g) is the weight of active materials on the Ni foam substrate and ΔV (V) is the potential window for a full discharge.

3 Results and discussion

The composition and crystal structure of the samples were studied by XRD. As shown in Fig. 1, GO appears a well-defined diffraction peak around 10.4°, which corresponds to the (001) crystal planes. After thermal treatment at 300 °C in argon for 4 h, the peak located at 10.4° disappears, and is replaced by two broad peaks around 24.8° and 42.5°, which are indexed to be the disorderedly stacked rGO sheets. In the XRD pattern of the GO/Ni$(HCO_3)_2$, the well-defined diffraction peaks appear at 14.9°, 26.0°, 33.8°, 37.1°, 40.2°, 43.1° and 45.9° (PDF#39-0316), indicating that the sample is composed of Ni $(HCO_3)_2$. After thermal treatment at 300 °C in argon for 4 h, the peaks associated with Ni$(HCO_3)_2$ completely disappear, a series of peaks at 37.2°, 43.2°, 62.8°, 75.2° and 79.4° corresponding to the cubic NiO, which are ascribed to the (111), (200), (220), (311) and (222) crystal planes, respectively, The XRD diffraction peaks of rGO/NiO shift to the small angle direction compared to NiO, indicating that the interlayer distance is enlarged due to the incorporation of rGO. The restacking diffraction peaks of GO or rGO are absent in GO/Ni $(HCO_3)_2$ and rGO/NiO, indicating that the uniform distributed Ni $(HCO_3)_2$/NiO on both sides of the GO/rGO sheets prevents the restacking of GO/rGO sheets.

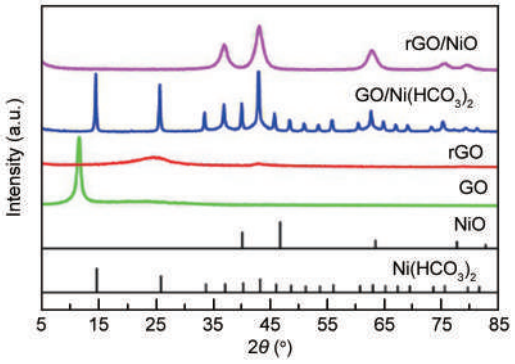

Fig. 1　XRD patterns of the samples.

The morphology and microstructure of GO/Ni $(HCO_3)_2$ and rGO/NiO are shown in Fig. 2. It can be seen that the as-prepared materials are consisted of irregular particles and these particles stack randomly to form agglomerates. For GO/Ni$(HCO_3)_2$, a dense morphology is observed (Fig. 2a, b). rGO/NiO presents the looser morphology than GO/Ni $(HCO_3)_2$. The loose structure ensures the diffusion of electrolyte ions into the bulk phase of electrode ma-

terials and improves the accessible surface area of the composite, leading to the enhanced electrochemical performances[22, 23].

The specific surface area and porous structure of the as-prepared samples were further investigated by nitrogen adsorption. The nitrogen adsorption/desorption isotherms of the samples present a typical IV isotherm with a H3 hysteresis loop at the relative pressure of 0.4-0.98, suggesting a meso- and macroporous structure. The corresponding specific surface areas and pore volumes are 105.7 $m^2\ g^{-1}$, 0.23 $cm^3\ g^{-1}$ and 121.3 $m^2\ g^{-1}$, 0.26 $cm^3\ g^{-1}$ for GO/Ni(HCO_3)$_2$ and rGO/NiO, respectively. GO/Ni(HCO_3)$_2$ possesses a narrow mesoporous distribution about 3-4 nm. Whereas, rGO/NiO possesses a hierarchical pore size distribution around 2-100 nm and the pore size mainly appears at 10-60 nm. During the thermal treatment process, CO_2 and H_2O generated by the decomposition of Ni(HCO_3)$_2$ can act as a pore-forming agent to promote the formation and the enlargement of pores. Thus, a loose structure with a hierarchical porous distribution is obtained for rGO/NiO. Generally, micro- and mesopores provide a high surface area, which result in a large capacitance. Macropores can shorten the ions diffusion distance and act as the ion-buffering reservoirs. The network structure of rGO can enhance the electronic conductivity and improve the electrochemical stability[24].

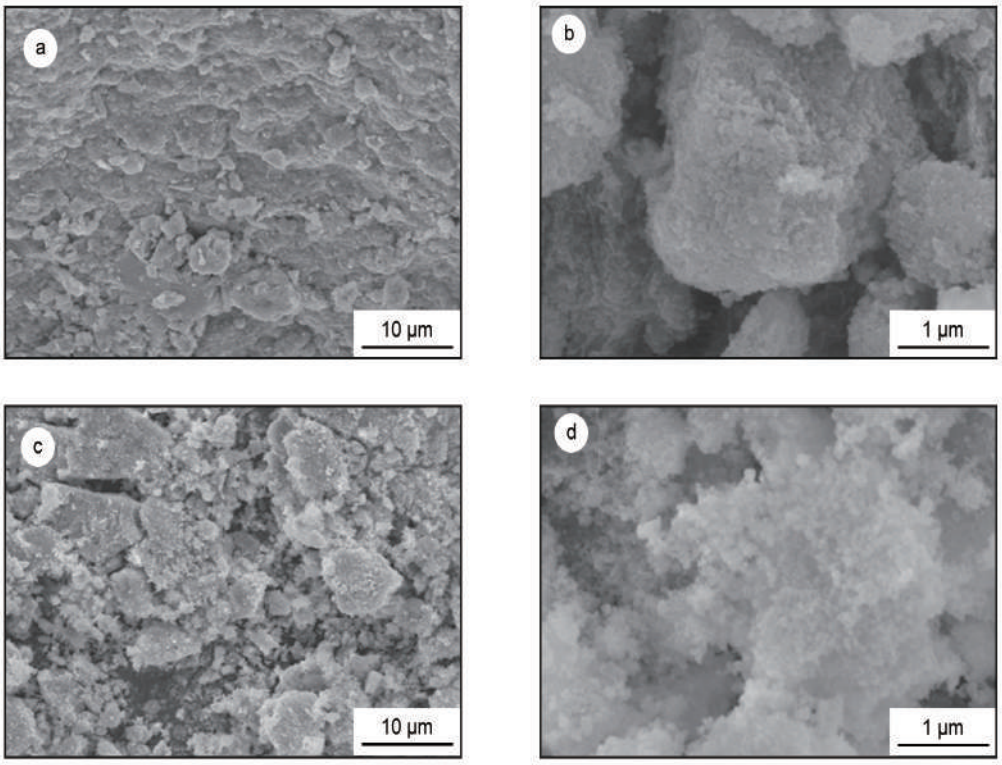

Fig. 2 SEM images of (a, b) GO/Ni(HCO_3)$_2$ and (c, d) rGO/NiO.

Table 1 BET surface areas and pore parameters of the obtained samples.

Samples	BET surface areas ($m^2\ g^{-1}$)	Pore volume ($cm^3\ g^{-1}$)	Micropore volume ($cm^3\ g^{-1}$)	Average pore diameter (nm)
GO/Ni(HCO_3)$_2$	105.7	0.23	0.0032	8.75
rGO/NiO	121.3	0.26	0.0026	8.69

The weight percentage of NiO in the composites was estimated by TG in air. As shown in Fig. 4, rGO/NiO exhibits a small mass loss of 8.5% at the temperature less than 200 °C, which is attributed by the removal of the adsorbed water. The obvious mass loss between 300 and 400 °C is due to the thermal decomposition of rGO. After 600 °C, the TG curve tends to be stable without any further obvious weight loss, indicating the decomposition of rGO is completed. The residual weight ratio is the content of NiO in the rGO/NiO composite. Therefore, the percentage of the NiO in the composite is about 49 wt%.

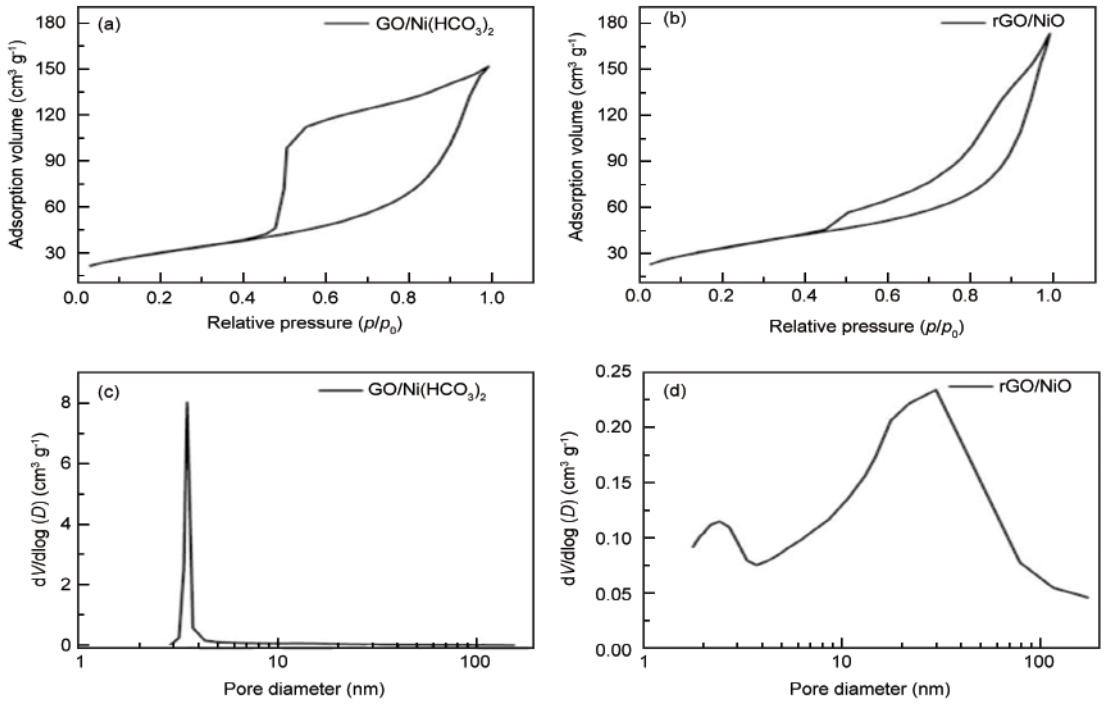

Fig. 3　(a,b) Nitrogen adsorption/desorption isotherms and (c,d) pore size distributions of samples.

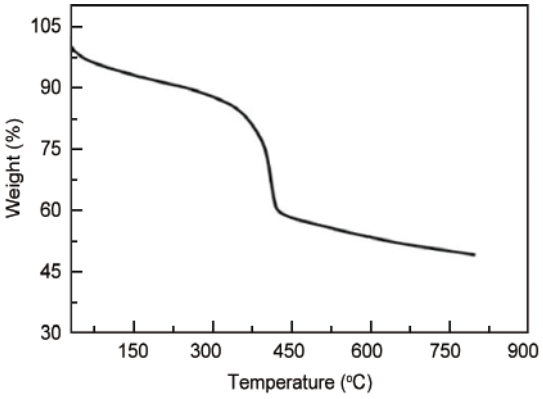

Fig. 4　TG curve of rGO/NiO.

The electrochemical performance of rGO/NiO composite was evaluated by CV and CD measurements in a three-electrode system using 2 mol L^{-1} KOH as the electrolyte. As a comparison, CV and CD curves of the pure NiO were measured under the same conditions. Fig. 5a shows the CV curves of the as-prepared samples. A pair of redox peaks correspond to the reversible reactions of Ni^{2+} and Ni^{3+}, indicating that the capacitance of the samples mainly arises from the pseudocapacitive behavior of NiO based on the redox mechanism. The redox mechanism of NiO is expressed by the following reaction[25]:

$$NiO + OH^- \rightleftharpoons NiOOH + e^- \quad (2)$$

rGO/NiO presents the larger enclosed areas, indicating a higher specific capacitance than that of NiO. The specific capacitances are 437, 919 F g^{-1} for pure NiO and rGO/NiO, respectively, according to the CD curves at the current density of 0.5 A g^{-1}. Rate capability is important for supercapacitors. The CD curves at the different current densities are shown in Fig. 5c, d. The specific capacitances are 437, 368, 327, 248 F g^{-1} for NiO and 919, 781, 696, 648 F g^{-1} for rGO/NiO at the current density of 0.5, 1, 2, 5 A g^{-1}, respectively. The specific capacitance retention rate is 57% and 71% when the current densities increase from 0.5 to 5 A g^{-1}. The enhanced electrochemical performance is mainly related to the micro structure. The higher specific surface area of rGO/NiO allows exposing more surfaces to the electrolyte and provides a large amount of electroactive sites for redox reactions. On the other hand, the intercalation between NiO nanosheets and rGO nanosheets prevents the re-aggregation of NiO nanosheets and the restacking of rGO nanosheets and improves their utilization ratio. Besides, the incorporation of rGO and the optimal porous distribution enable the fast electron transfer and the fast ion diffusion, which results in higher specific capacitance and enhanced rate capability[26]. The CV profiles (Fig. 5e, f) clearly exhibit the similar redox couples at the different scan rates. As the scan rates increase, the response current increase and the shapes of the CV curves tend to be asymmetric and polarized because the limited ion diffusion rate is unable to satisfy electronic neutralization during the redox reaction[27]. The Randles-Sevcik plots show the relationship between

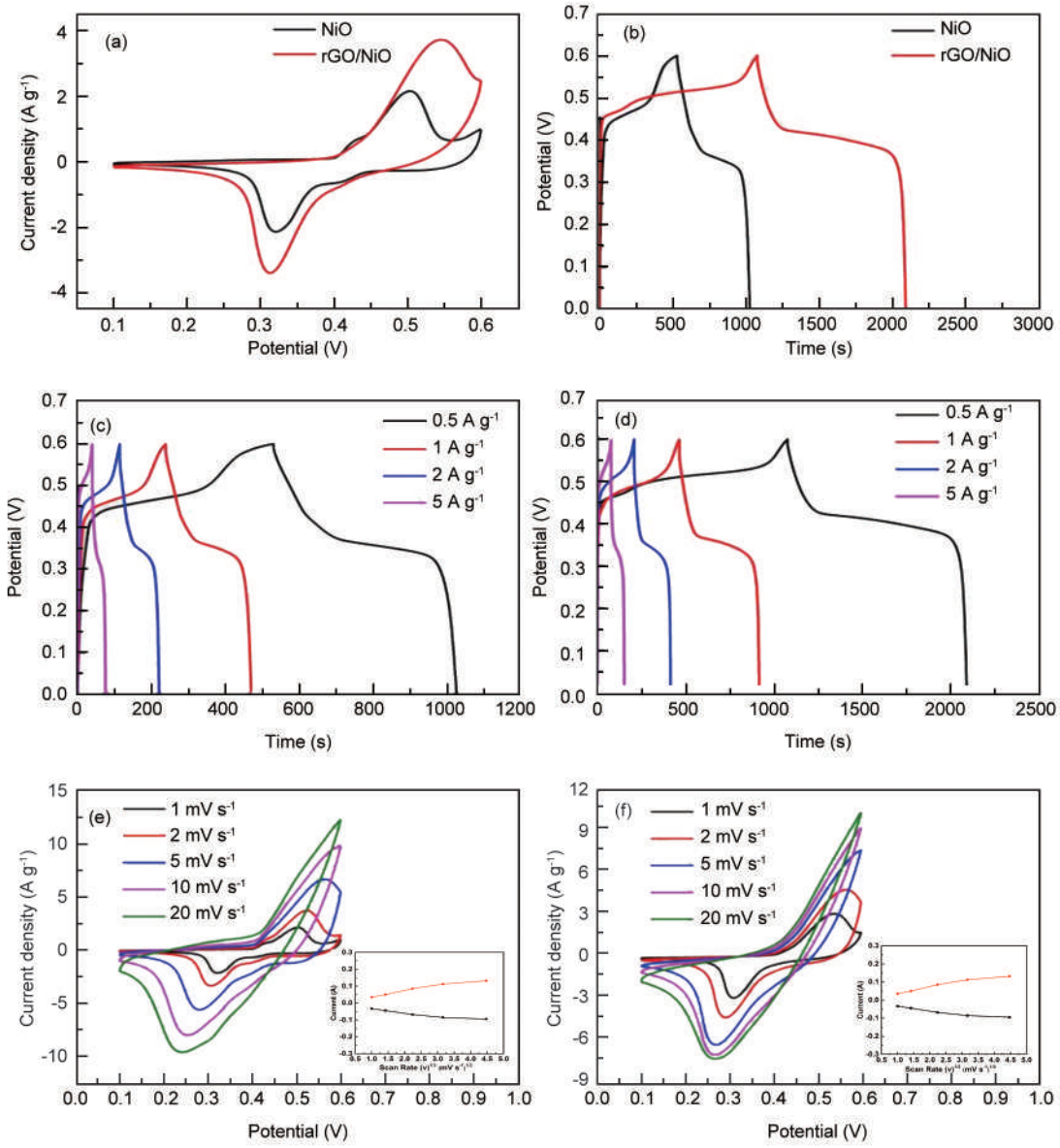

Fig. 5 Electrochemical performance: (a) CV curves at the scan rate of 2 mV s^{-1}, (b) CD curves at the current density of 0.5 A g^{-1}, (c) CD curves of NiO, (d) CD curves of rGO/NiO, (e) CV curves and Randles-Sevcik plots of NiO, and (f) CV curves and Randles-Sevcik plots of rGO/NiO.

the peak currents and the square root of the scan rate. The electrochemical processes are diffusion controlled for the electrodes according to the results of Randles-Sevcik plots (inset in Fig. 5e, f).

EIS was also performed to understand the ion diffusion and electrochemical kinetics during charging. Fig. 6a shows the EIS plots of pure NiO and of rGO/NiO. Each plot is consisted of a depressed semicircle at high frequency and a linear part at low frequency. Generally, the intercept of the curves with the real axis at high frequencies represents the equivalent series resistances (*R*s) of the electrode, which includes the inherent resistance of electrode material, bulk resistance of the electrolyte solution, and contact resistance at the active material/current collector interface. The semi-circles display the charge transfer resistance (*R*ct) caused by the Faradaic reactions and the double-layer capacitance at the working electrode/electrolyte interface, whereas the straight line corresponds to the ion diffusion of the electroactive materials (Zw)[28]. The estimated *R*s values are about 0.62 and 0.59 Ω for the pure NiO and rGO/NiO, respectively. The corresponding *R*ct values are 0.66 and 0.48 Ω according to the diameter of the depressed semicircles. The decrease of *R*s and *R*ct is due to the incorporation of rGO, which improves the conductivity of electrode materials. It is clear that rGO/NiO exhibits a smaller Zw than that of pure NiO, indicating the fast ion diffusion process. The long-term cycling sta-

bility of rGO/NiO is also recorded at the current density of 2 A g^{-1}, as shown in Fig. 6b. The specific capacitance decreases from 696 to 633 F g^{-1}, with a 91% capacitance retention ratio, demonstrating the excellent cycle stability. It is well known that the capacity decay is caused by the aggregation and pulverization of electrode materials accompanying the charge/discharge process. The electrochemical performance of rGO/NiO is compared with previous reported literatures (Table 2). As shown in Table 2, rGO/NiO presents the enhanced electrochemical performance due to the incorporation of rGO and the formation of the hierarchical porous structure.

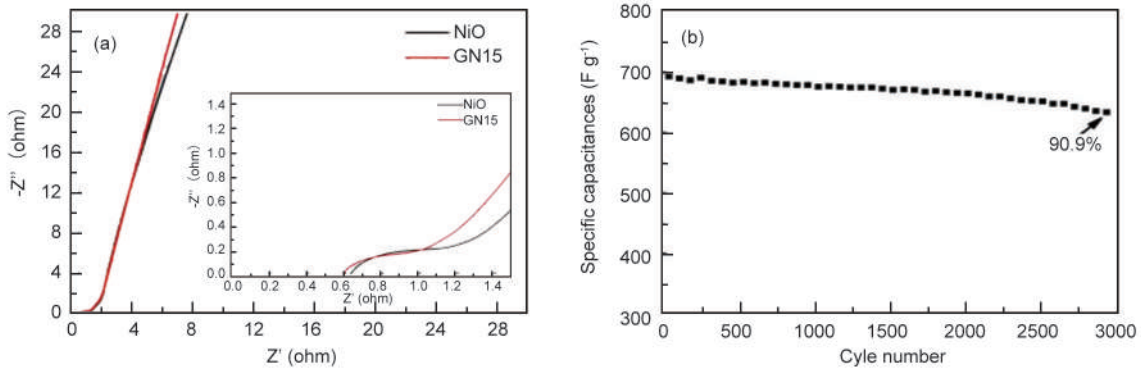

Fig. 6 (a) Nyquist curves of the samples and (b) Cycling stability test of rGO/NiO.

Table 2 The comparison of the electrochemical performances of various rGO/NiO.

The specific capacitances	The specific capacitance retention	The long-term cycling stability	The weight percentage of NiO	Ref.
1161 F g^{-1} (2 A g^{-1})	72.3% (2-10 A g^{-1})	92% (3000 cycles)		[14]
871 F g^{-1} (1 A g^{-1})	–	89% (3000 cycles)	–	[10]
877 F g^{-1} (1 A g^{-1})	–	90% (1000 cycles)		[11]
585 F g^{-1} (1 A g^{-1})	50.4% (1-10 A g^{-1})	100% (6000 cycles)	85%	[29]
919 F g^{-1} (0.5 A g^{-1})	70.5% (0.5-5A g^{-1})	91% (3000 cycles)	49%	This work

4 Conclusions

GO/Ni$(HCO_3)_2$ composite was synthesized by heterogeneous self-assembly, followed by thermal treatment to obtain rGO/NiO. rGO/NiO presents the higher specific surface areas of 121.3 m^2 g^{-1} and bigger pore volumes of 0.26 cm^3 g^{-1} than those of GO/Ni$(HCO_3)_2$. rGO/NiO possesses a hierarchical porous distribution around 2-100 nm due to the releasing of generated CO_2 and H_2O. Compared with GO/Ni$(HCO_3)_2$, the higher specific surface area and the hierarchical porous distribution endow rGO/NiO composite with a higher specific capacitance of 919 F g^{-1} (0.5 A g^{-1}) and improved rate capability of 71% when the current density increase from 0.5 to 5 A g^{-1}. The result of the long-term cycling stability shows that the specific capacitance retention of 91% is obtained after 3 000 cycles.

References

[1] Zhou Q Y, Fan T W, Li Y Y, et al. Hollow - structure NiCo hydroxide/carbon nanotube composite for High-Performance supercapacitors [J]. Journal of Power Sources, 2019, 426: 111-115.

[2] Yu C, Xu F, Luo L, et al. Bimetallic Ni-Co phosphide nanosheets self-supported on nickel foam as high-performance electrocatalyst for hydrogen evolution reaction [J]. Electrochimica Acta, 2019, 317: 191-198.

[3] Liu Y, Guo S J, Zhang W, et al. Three-dimensional interconnected cobalt sulfide foam: Controllable synthesis and application in supercapacitor [J]. Electrochimica Acta, 2019, 317: 551-561.

[4] Yuan S X, Lu C X, Li Y, et al. Two-step deposition/reduction synthesis of porous lamellar Ni$(OH)_2$/reduced graphene oxide composites with large capacitance for supercapacitors [J]. ChemElectroChem, 2017, 4 (11): 2826-2834.

[5] Pourfarzad H, Shabani N M, Ganjali M R, et al. Synthesis of Ni-Co-Fe layered double hydroxide and Fe_2O_3/graphene nanocomposites as actively materials for high electrochemical performance supercapacitors [J]. Electrochimica Acta, 2019, 317: 83-92.

[6] Yang P H, Qu X P, Liu K, et al. Electrokinetic supercapacitor for simultaneous harvesting and storage of mechanical energy [J]. ACS applied materials & interfaces, 2018, 10(9): 8010-8015.

[7] Ishaq M, Jabeen M, Song W M, et al. Fluorinated graphene – supported nickel-cobalt-iron nitride nanoparticles as a promising hybrid electrode for supercapacitor applications [J]. Electrochimica Acta, 2018, 282: 913-922.

[8] Xiao C Y, Zhang W L, Lin H B, et al. Modification of a rice husk-based activated carbon by thermal treatment and its effect on its electrochemical performance as a supercapacitor electrode [J]. New Carbon Materials, 2019, 34(4): 341-348.

[9] Wei F, Zhang H F, He X J, et al. Synthesis of porous carbons

from coal tar pitch for high-performance supercapacitors [J]. New Carbon Materials, 2019, 34(2): 132-139.

[10] Roy A, Ray A, Saha S, et al. NiO-CNT composite for high performance supercapacitor electrode and oxygen evolution reaction [J]. Electrochimica Acta, 2018, 283: 327-337.

[11] Das M R, Roy A, Mpelane S, et al. Influence of dipping cycle on SILAR synthesized NiO thin film for improved electrochemical performance [J]. Electrochimica Acta, 2018, 273: 105-114.

[12] Li Q, Wei Q, Xie L J, et al. Layered NiO reduced graphene oxide composites by heterogeneous assembly with enhanced performance as high-performance asymmetric supercapacitor cathode [J]. RSC Advances, 2016, 6: 46548-46557.

[13] Zhi M J, Xiang C C, Li J T, et al. Nanostructured carbon-metal oxide composite electrodes for supercapacitors: A review [J]. Nanoscale, 2013, 5(1): 72-88.

[14] Liu P B, Yang M Y, Zhou S H, et al. Hierarchical shell-core structures of concave spherical NiO nanospines@ carbon for high performance supercapacitor electrodes [J]. Electrochimica Acta, 2019, 294: 383-390.

[15] Yus J, Bravo A J, Sanchez H, et al. Electrophoretic deposition of RGO-NiO core-shell nanostructures driven by heterocoagulation method with high electrochemical performance [J]. Electrochimica Acta, 2019, 308: 363-372.

[16] Nunes W G, Da S L M, Vicentini R, et al. Nickel oxide nanoparticles supported onto oriented multi-walled carbon nanotube as electrodes for electrochemical capacitors [J]. Electrochimica Acta, 2019, 298: 468-483.

[17] Bai J W, Yan H J, Liu Q, et al. Synthesis of layered α-Ni $(OH)_2$/RGO composites by exfoliation of α-Ni $(OH)_2$ for high-performance asymmetric supercapacitors [J]. Materials Chemistry and Physics, 2018, 204: 18-26.

[18] Ansy K M, Lee J H, Piao H Y, et al. Stabilization of antioxidant gallate in layered double hydroxide by exfoliation and reassembling reaction [J]. Solid State Sciences, 2018, 80: 65-71.

[19] Zang X X, Dai Z Y, Guo J, et al. Controllable synthesis of triangular Ni $(HCO_3)_2$ nanosheets for supercapacitor [J]. Nano Research, 2016, 9(5): 1358-1365.

[20] Zhao S Q, Wang Z W, He Y J, et al. Interconnected Ni $(HCO_3)_2$ hollow spheres enabled by self-sacrificial templating with enhanced lithium storage properties [J]. ACS Energy Letters, 2016, 2(1): 111-116.

[21] Tian J J, Xue Y, Wang M M, et al. Dopamine constructing composite of Ni $(HCO_3)_2$-polydopamine-reduced graphene oxide for high performance electrode in hybrid supercapacitors [J]. Electrochimica Acta, 2019, 296: 49-58.

[22] Bhojane P, Sinha L, Goutam U K, et al. A 3D mesoporous flowers of nickel carbonate hydroxide hydrate for high-performance electrochemical energy storage application [J]. Electrochimica Acta, 2019, 296: 112-119.

[23] Liang H Y, Lin J H, Jia H N, et al. Hierarchical NiCo-LDH@ NiOOH core-shell heterostructure on carbon fiber cloth as battery-like electrode for supercapacitor [J]. Journal of Power Sources, 2018, 378: 248-254.

[24] Li Y Y, Li Z S, Shen P K. Simultaneous formation of ultrahigh surface area and three-dimensional hierarchical porous graphene-like networks for fast and highly stable supercapacitors [J]. Adv Mater, 2013, 25(17): 2474-2480.

[25] Feng X S, Huang Y, Li C, et al. Controllable synthesis of porous $NiCo_2O_4$/NiO/Co_3O_4 nanoflowers for asymmetric all-solid-state supercapacitors [J]. Chemical Engineering Journal, 2019, 368: 51-60.

[26] Geuli O, Hao Q L, Mandler D. One – step fabrication of NiOx-decorated carbon nanotubes-$NiCo_2O_4$ as an advanced electroactive composite for supercapacitors [J]. Electrochimica Acta, 2019, 318: 51-60.

[27] Wang N, Han G Y, Chang Y Z, et al. Preparing Ni_3S_2 composite with neural network-like structure for high-performance flexible asymmetric supercapacitors [J]. Electrochimica Acta, 2019, 317: 322-332.

[28] Urhan B K, Demir ü. Electrochemical fabrication of Ni or Ni $(OH)_2$@ Ni nanoparticle-decorated reduced graphene oxide for supercapacitor applications [J]. Electrochimica Acta, 2019, 302: 109-118.

[29] Liu T, Jiang C J, Cheng B, et al. Hierarchical flower-like C/NiO composite hollow microspheres and its excellent supercapacitor performance [J]. Journal of Power Sources, 2017, 359: 371-378.